Chiral Periodic Mesoporous Organosilica in a Smectic-*A* Liquid Crystal: Source of the Electrooptic Response

Ian R. Nemitz[a], Kevin McEleney[b], Cathleen M. Crudden[b], Robert P. Lemieux[c], Rolfe G. Petschek[a], and Charles Rosenblatt[a,1]

[a]*Department of Physics, Case Western Reserve University, Cleveland, Ohio 44106 USA;*
[b]*Department of Chemistry, Queen's University, Kingston, Ontario, Canada K7L 3N6;*
[c]*Department of Chemistry, University of Waterloo, Waterloo, Ontario, Canada N2L 3G1*

(Received; accepted)

Abstract

Chiral periodic mesoporous organosilica (PMO) materials have been shown to deracemize a configurationally achiral, but conformationally racemic liquid crystal in which the PMO is embedded. In particular, application of an electric field *E* in the liquid crystal's smectic-*A* phase results in a rotation of the liquid crystal director by an angle proportional to *E*, which is detected optically — this is the so-called "electroclinic" effect. Here we present results from electroclinic measurements as a function of frequency and temperature, which allow us to distinguish the component of optical signal that arises from liquid crystal chirality induced within the PMO's chiral pores from that induced just outside the silica colloids. Our central result is that the overwhelming source of our electrooptic signal emanates from outside the PMO, and that the contribution from the liquid crystal embedded in the chiral pores is much smaller and below the noise level.

Graphical Abstract: TEM image of PMO showing the 2D hexagonally ordered porous mesostructured

Keywords: PMO, electroclinic, smectic-A, chiral

[1] Corresponding author. Email: rosenblatt@case.edu

1. Introduction

Infiltration of liquid crystals into porous materials has provided insight into phase transitions in confined geometries [1]. Recently, such systems have presented a variety of potential applications, including electrooptics (such as controllable photonic band-gap materials) [2] and energy-harvesting [3,4]. The development during the past decade of periodic mesoporous organosilicas (PMOs, Fig. 1) has caused a stir in the scientific community [5,6,7,8,9,10,11,12]. PMO microparticles are prepared by the surfactant-templated condensation of bridged organosilsesquioxane monomers [11]. PMOs are thus unique among other silica-based porous materials since the inclusion of an organic unit directly within the walls of the material provides the opportunity to exert significant control over the structure and properties of the resulting composition material. In addition, by judicious choice of surfactant and condensation conditions, the PMO can be tailored to have an extensive range of chemical and physical properties, including nanometer sized pores and controlled spacing of the highly ordered porous channels. The use of bridging *chiral* monomers provides the unique opportunity to impart chirality into the backbone of the material, including within the PMO pores, facilitating possible applications in chiral chromatography and non-linear optics [12].

To date, only a few reports have appeared that characterize the chirality of pore structures in these materials. Characterization of chirality has been achieved by methods including polarimetry [13,14], solid-state circular dichroism [15], interactions with chiral gases [16] and the interactions of chiral PMOs with liquid crystalline solvents [11]. In particular, suspension of micrometer-sized chiral PMO particles in a configurationally achiral liquid crystal matrix, and the resulting infiltration of the liquid crystal into the PMO pores, has been shown to induce measurable chiral properties in the nematic and smectic-*A* (Sm-*A*) phases of liquid crystals [11]. For example, a 90^0 nematic twist cell filled with the configurationally achiral liquid crystal 4-cyano-4'-pentylbiphenyl

(5CB) doped with chiral PMO particles displays bowed disclination lines in the bulk liquid crystal [11]. This behavior indicates that the liquid crystal has been partially deracemized conformationally so that domains having the same imposed handedness of twist as the deracemized liquid crystal are favored at the expense of the opposite sense of twist [17]. Importantly, this result also shows that the chiral pores induce chirality in the liquid crystal *outside* the PMO. In the same paper [11] it was shown that a cell containing a mixture of the conformationally racemic liquid crystal **9OO4** (**1**, Fig. 2) in its Sm-*A* phase and chiral PMO microparticles exhibits an electroclinic effect (ECE), in which application of an electric field E induces a rotation θ of the liquid crystal director $\hat{n}$, where $\theta \propto E$ [18]. Moreover, the proportionality constant between θ and E can be taken as a measure of the chiral strength. Chirality is a requirement for the appearance of this electroclinic effect.

The appearance of these chiral signatures in the nematic cell clearly demonstrates that chiral PMO induces chirality — directly or indirectly —in the interparticle region of the liquid crystal, outside the PMO pores. Importantly, Jayalakshmi, *et al.*, showed that the chiral electroclinic signature vanishes if the PMO pores are plugged with an achiral surfactant that prevents pore infiltration by the liquid crystal [11]. From this result, it was concluded that the chirality transfer to the bulk achiral liquid crystal originates predominantly from within the pores. These results suggest that the chiral pores deracemize the liquid crystal in the filled pores, and that chirality is transferred to the bulk of the liquid crystal through interactions at the mouth of the pores. However, in our previous study, the contribution of the liquid crystal within the pores to the overall electrooptical signature was not separated from that attributed to the bulk phase. Thus, herein we present electroclinic measurements in the Sm-*A* phase of **9OO4** doped with chiral PMO particles as a function of angular frequency ω of the applied electric field and of temperature T above the Sm-*A* –

Sm-*C* phase transition temperature $T_{AC,}$ which allows us to separate the effect of the encapsulated liquid crystal from that of the bulk exterior liquid crystal.

2. Experimental

The optically pure (*S*) chiral binaphthyl monomer **2** (Fig. 2) — this is similar, but not identical, to the binaphthyl-based monomer used in Ref. 11 — was co-condensed with the bulk monomer 4,4'-bis-(triethoxysilyl)biphenyl (**3**, Fig. 2) to prepare the chiral PMO materials. The nonionic, alkylpolyether surfactant Brij 76 was chosen for co-condensation using a mixture of **2** and **3** in an 85 : 15 (w/w) ratio. The templating surfactant was removed after co-condensation by Soxhlet in acidic ethanol, leaving mesoporous particles of (S)-**15-QPMO1-ex** having a range of aspect ratios, but of characteristic size $d \sim 1$ μm. The particles contain well-ordered pores of diameter ~ 2.5 nm in a hexagonal lattice with spacing ~ 6 nm. Details of the synthesis are described elsewhere [19].

The liquid crystal **9OO4**, whose phase sequence for this batch was measured to be Crystal – 34 – Smectic-B – 44 – Sm-C – 57.5 – Sm-A – 70 – Nematic – 85.5 – Isotropic, was mixed with the PMO particles in toluene, rendering a final concentration of 1.0 wt.-% PMO in liquid crystal after the solvent was removed by evaporation. Cells were constructed using a pair semi-transparent, electrically-conducting indium-tin-oxide (ITO) coated glass substrates. The ITO was spin-coated with the polyamic acid RN-1175 (Nissan Chemical Industries), baked according to manufacturer's specifications, *i.e.*, 5 min at 80°C then 1 h at 250°C to imidize, and then rubbed unidirectionally with a cotton pile cloth (YA-20-R, Yoshikawa Chemical Co.) to create an easy axis for planar liquid crystal director alignment. The substrates were then placed together with the rubbing directions oriented antiparallel, separated by Mylar spacers, and cemented. Housed inside an Instec 402 temperature controller with stability of a few millikelvins, the cell was filled in the bulk isotropic phase with the (*S*)-**15-QPMO1-ex / 9OO4** mixture. For comparison purposes, a second cell was

constructed and filled with a 0.56 wt.-% mixture of the chiral molecular dopant **CB15** (**4**, Merck, Fig. 2) in **9OO4**; this chiral dopant facilitated an ECE without the imposition of micron-sized PMO inclusions. The thickness d of each cell cavity was determined by optical interference before the cell was filled. d was found to be (10.0 ± 0.1) μm for the PMO-containing cell and (3.9 ± 0.2) μm for the **CB15** containing cell.

Similar measurements described forthwith were performed separately on each of the two samples. Each cell was cooled from the isotropic phase and the temperature was stabilized in the Sm-*A* phase. We used the classical electroclinic geometry [20] to measure an effective electroclinic coefficient $e_c = d\theta / dE$ *vs.* frequency and temperature. Light from a He-Ne laser passed consecutively through a polarizer oriented at 22.5° with respect to cell's rubbing direction, the cell, and then through a crossed polarizer before passing into a fast photodiode detector. The detector's output was fed into a preamplifier and then into a lock-in amplifier that was referenced to the angular frequency ω of the electric field applied across the cell. (The detector and preamplifier's responses were flat to well over 6.28×10^5 s^{-1}, *i.e.,* > 100 kHz.) Measurements were made in the lock-in amplifier's *R*-θ mode, *i.e.,* the amplitude and phase of the signal. In this geometry it can be shown [20] that the effective induced director rotation $\theta = I_{ac} / 4I_{dc}$, where I_{ac} is the measured amplitude of the intensity at frequency ω and I_{dc} is the dc intensity. θ corresponds to the actual director rotation for a well-aligned Sm-*A* cell, such as the cell containing **CB15**; however, here θ corresponds to an effective director rotation averaged over the 1 mm diameter laser spot for a cell that contains PMO microparticles with not-well-defined director boundary conditions at the PMO surface. This will be discussed in more detail later.

First we verified that the experimental set-up was working properly by examining the **CB15** / **9OO4** sample at three temperatures: T = 59°, 60°, and 62°C. An ac voltage at ω = 628 s^{-1} (100 Hz) was applied to the cell and increased step-wise from zero to 10 V rms over 1200 s, with a dwell

time of 15 s at each applied voltage setting. Because of the relatively weak signal-to-noise ratio, the lock-in amplifier's time constant was set at 3 s. We found that $\theta = I_{ac} / 4I_{dc}$ is linear in voltage V, as shown in Fig. 3; moreover, no hydrodynamic instabilities were observed at these voltages. Given the linear response, we then fixed the applied voltage at 7 V rms and measured $\theta \left[= I_{ac} / 4I_{dc}\right]$ for the **CB15 / 9OO4** sample as a function of frequency ω over the range $250 \leq \omega \leq 6.28 \times 10^5$ s^{-1}. (Measurements at $\omega < 250$ s^{-1} were found to be noisy and less reliable, particularly for ΔT $\left[\equiv T - T_{AC}\right] > 1^{\circ}$C, and therefore will not be used in the analysis and discussion.) Data were collected in intervals of approximately 50 mK above the Sm-A – Sm-C transition. Figure 4 shows θ vs. ω with 7 V rms applied at several representative temperatures ΔT in the Sm-A phase close to T_{AC}. The transition temperature $T_{AC} = (57.52 \pm 0.02)\ ^{\circ}$C was taken to be the temperature at which $d\theta / dE$ saturates at $\omega = 628$ s^{-1}. The experiment was then repeated using the **(S)-15-QPMO1-ex** (PMO) / **9OO4** mixture, and representative results are shown in Fig. 5.

3. Discussion

Let us first consider the **CB15 / 9OO4** data in Fig. 4, which correspond to a bulk, electroclinic effect in the Sm-A phase. In the equal elastic constant approximation, the free energy density F in the Sm-A phase can be written

$$F = \tfrac{1}{2} K \left(\nabla \theta\right)^2 + \tfrac{1}{2} D\theta^2 - cE\theta \,, \qquad (1)$$

where D is the inverse tilt susceptibility of the director in the Sm-A phase and which vanishes as $T \rightarrow T_{AC}$, c is the coupling constant between θ and E in the free energy, and K is an elastic constant in the Sm-A phase that tends to inhibit spatial variations of the director. On spatially Fourier transforming Eq. 1 and using the dynamical equation for θ_q, *viz.*, $\eta \partial \theta_q / \partial t = -\partial F / \partial \theta_q$, where η is a

viscosity, θ_q is the spatial Fourier component of the rotation angle, and q is the wavevector, we obtain

$$\eta \frac{d\theta_q}{dt} + D\theta_q + Kq^2\theta_q = cE \tag{2}$$

Whence the magnitude of the Fourier component of the field-induced director rotation at frequency ω is

$$\theta_q = cE / \left[\left(D + Kq^2 \right)^2 + \omega^2\eta^2 \right]^{1/2} \tag{3}$$

For the **CB15 / 9OO4** cell we can estimate the importance of the different terms by taking η ~ 0.1 kg m^{-1} s^{-1}, K ~ 10^{-11} N [21], and q ~ 10^6 m^{-1}, *i.e.,* π divided by the cell thickness. (This value for q assumes a director orientation that is fixed along the easy axes at the cell's walls. This is unlikely to occur, and q is likely to be smaller than 10^6 m^{-1}). Well above T_{AC}, the inverse tilt susceptibility term D is large [22] and totally dominates the denominator up to frequencies ω ~ 10^5 s^{-1}. Close to T_{AC} the D term becomes small and vanishes at T_{AC}. In this region, we need to compare the K^2q^4 term with the $\omega^2\eta^2$ term. Even at a low frequency ω ~ 300 s^{-1} we calculate that the elastic term << the viscous damping term. From these comparisons, we see that the q-dependent term in Eq. 3 can be neglected entirely for the **CB15 / 9OO4** cell. Thus, for this mixture the simple model predicts that $\theta_q \approx cE / \left(D^2 + \omega^2\eta^2 \right)^{/2}$ at all frequencies and temperatures studied in this work.

Using this Debye form, we fitted the data in Fig. 4 using two fitting parameters, D/c and η/c; the results from the two fits are shown in Figs. 6a and 6b. The fits are very good close to T_{AC} but as the temperature is increased, the experimental data become slightly stretched along the frequency

axis relative to the Debye form. Using the ferroelectric mixture SCE12 (Merck), Li, *et al.*, observed an anomalous relaxation time at higher temperatures in the Sm-*A* phase [23]. They proposed that the ECE can be described by *two* coupled dynamical equations, the dynamical equation above involving θ and another involving the induced polarization P, *viz.,* $\eta \partial P_q / \partial t = -\partial F / \partial P_q$. This produces an eigenvalue equation whose solution has a slow and a fast mode. The ECE experiment probes a combination of the two modes, such that $d\theta / dE$ is a linear combination of the slow and fast mode Debye-like responses. [We remark that dP / dE is a (different) linear combination of the same slow and fast processes.] Close to T_{AC}, the slow response dominates $d\theta / dE$ with only a negligible contribution from the fast process; thus our fit to a single Debye process is quite good in this temperature regime. At higher temperatures, however, Li, et al suggested [23] that the fast mode comes to play a more important role in $d\theta / dE$, thereby explaining the observed stretch of the measured ECE along the frequency axis. Thus, absent a much more detailed model, we will focus our measurements and discussion on the temperature region within $\Delta T = \sim 1^{o}$C of T_{AC} [24].

Now we consider Fig. 5, which shows the data from the PMO-containing sample, *i.e.,* the (*S*)**-15-QPMO1-ex / 9OO4** mixture. The data, which are much more stretched along the ω axis than the **CB15 / 9OO4** data at comparable values of ΔT, clearly are inconsistent with the Debye form of Eq. 3, even at small ΔT. We need to examine several sources for the observed chiral electroclinic signature. Previously we noted that a (*S*)**-15-QPMO1-ex / 9OO4** mixture in a 90^{o} twist nematic cell exhibits bowed disclination lines, from which the effective chiral pitch can be extracted [11]. This result suggests that one source of the ECE may occur in the bulk liquid crystal, outside the PMO pores. Earlier measurements, in which the PMO pores are plugged with an achiral surfactant before mixing the PMO particles into the liquid crystal, showed no signs of induced liquid crystalline chirality [11]. This means that the chiral induction outside the silica particle is not being caused by the silica surface, but rather the induction emanates from the liquid crystal-filled

chiral pores over some distance L — perhaps 5 or 10 nm [25] — into the bulk **9OO4**. We can model this behavior in real space by assuming that the liquid crystal outside the PMO becomes chiral in a thin region of thickness L where the pores exit from the silica. On application of an electric field, the liquid crystal director in this region undergoes a rotation and elastically induces a rotation of the bulk liquid crystal further away from the PMO. The free energy density $F_{achiral}$ in the achiral *bulk* liquid crystal is

$$F_{achiral} = \tfrac{1}{2} K \left(\nabla \theta\right)^2 + \tfrac{1}{2} D\theta^2 \quad , \tag{4}$$

Note that here there is no chiral coupling term containing the applied field in the bulk liquid crystal. Applying Euler's equation to $F_{achiral}$ and reintroducing a viscous term, we obtain

$$\eta \frac{\partial \theta}{\partial t} = K\nabla^2\theta - D\theta \quad . \tag{5}$$

On performing a time Fourier transform of Eq. 5 and assuming that $\theta \rightarrow 0$ far from the chiral surface, we find the general solution $\theta = A \exp\left(-z\sqrt{i\omega\eta + D/K}\right)$, where A is a constant that is determined by the boundary conditions and z is a generic distance from the chiral liquid crystalline layer at the PMO's outer surface. The torque boundary condition when the director is normal to the silica surface is given by

$$-K\left(\frac{\partial \theta}{\partial z}\right)_{surf} + DL\theta_{surf} = cLE \quad , \tag{6}$$

where θ_{surf} is the director rotation at the pore-exit boundary. For other director orientations the effective value of D would need to be adjusted accordingly. For an applied electric field at frequency ω, *viz*., $E = E_0 e^{i\omega t}$, we obtain a solution for $\theta(z,\omega)$

$$\theta(z,t) = \frac{cLE_0}{DL + K\sqrt{\dfrac{i\omega\eta + D}{K}}} e^{-z\sqrt{\frac{i\omega\eta+D}{K}}} e^{i\omega t} \tag{7}$$

If we examine the magnitude of $\theta(z,\omega)$ at the PMO surface, *i.e.,* $\theta_{surf}(\omega)$ at z =0, we find behavior similar, but not identical, to that of the Debye behavior used to model the **CB15 / 9OO4** mixture in Fig. 6 and Eq. 3. There are two primary differences. First, the surface-driven process in Eq. 7 has a longer tail at high frequencies than does Eq. 3. This is to be expected because the surface-driven behavior involves not only modes near q = 0, but also the entire range of wavevectors, with the larger wavevector components having a faster response. Qualitatively, this behavior is observed in a high frequency tail for the (S)**-15-QPMO1-ex / 9OO4** mixture in Fig. 5. But we need to be cautious here. The optics for the **CB15 / 9OO4** mixture geometry probes the actual rotation angle θ in the bulk sample when q is small. For the PMO sample in which θ can vary with position in the liquid crystal, however, the experimental data in Fig. 5 do not correspond to the magnitude of θ_{surf}, but rather to some sample-averaged rotation that is approximately proportional to the rotation near the PMO surface. But there is yet another complication for the PMO cell: The elastic constant K — generally this would be the twist modulus K_{22} or the bend modulus K_{33} — takes on different values depending on the direction of z relative to the cell's easy axis direction and the PMO surface. This will have the effect of further broadening the frequency response. A full three-dimensional calculation is beyond the scope of this work. Nevertheless, the main point is that the chiral-induced liquid crystal near the pores exiting from PMO surface responds to the applied electric field and the rotation elastically propagates into the bulk, resulting in a more spread out frequency response than a bulk Debye process.

Let us now examine the low frequency behavior of the PMO sample, Fig. 5. That the electroclinic response of the (*S*)**-15-QPMO1-ex / 9OO4** mixture does not yet saturate at the lower

frequencies suggests that there is a significant relaxation process that is even slower than the $q \sim 0$ electroclinic effect, which is approximated by the **CB15 / 9OO4** mixture. What might this be? One possibility is that there is a dissipative process that occurs in the induced chiral liquid crystal layer immediately at the surface of the PMO, but which is not reflected in Eqs. 5-7; this corresponds to the region of liquid crystal that couples to the applied electric field in Eq. 6. Separately, we currently are examining the electroclinic effect in the thin (~ 10-20 nm) "paranematic" region at a planar-orienting substrate in at temperatures above the bulk isotropic to chiral nematic phase transition temperature T_{N^*I}. Preliminary results indicate a relaxation time of ~ 1 ms at approximately $T = T_{N^*I} + 500$ mK [26], suggesting a viscous interaction of the thin paranematic layer with the substrate on one side of the layer and/or the bulk isotropic liquid crystal on the other. Nevertheless this is still considerably faster than the observed slow relaxations reported herein, and we do not believe that this behavior is responsible for the observed slow process.

Turning to effects directly related to the PMO, it is important to realize that the PMO pores are not arranged radially from the particle's center. Rather, the pores are templated by the lyotropic columnar phase that forms from the surfactant, resulting in long columns over length scales of micrometer(s). Thus, the particles are not only anisometric in shape, but also anisotropic both optically and electrically [27], with the anisotropies arising from the shape birefringence of the aligned pores, the alignment of the birefringent monomers that form the PMO, and the liquid crystal molecules within the pores. It is likely that the pores' optical shape birefringence is relatively small due to the reasonably close refractive index match between the liquid crystal and silica. For an order of magnitude estimate of the PMO rotational contribution, we make the simple assumption that the PMO particles are uniaxial; thus the free rotational diffusion time $\tau_{free} = 1/6D_{rot}$ where D_{rot} is the rotational diffusion constant [28]. Even though there is a distribution of PMO particle shapes, in the spirit of this order of magnitude estimate we take $D_{rot} \sim k_B T / \pi \mu d^3$, where k_B is Boltzmann's

constant and μ is the shear viscosity. Here $d \sim 1$ μm. The shear viscosity μ is unknown owing to the likelihood of disordered smectic layers in contact with, at least, parts of the PMO surface. (We note, in fact, that the breaking and reconstruction of smectic layers as a result of the electric field itself and/or the rotation of the PMO also may contribute to the measured signal, with its own relaxation time.) Nevertheless, if we assume that $\mu \sim 0.1$ kg m^{-1} s^{-1}, we obtain a rotational random walk time $\tau_{free} \sim 10$ s. This suggests the presence of a slow process that may be observed optically due to the optical anisotropy of the PMO particles. Now, if we consider an *electrically-driven rotation* with a relaxation time $\tau_{driven} \sim 2k_B T / \varepsilon_0 \Delta\varepsilon_{PMO} E^2 d^3 D_{rot}$, where ε_0 is the permittivity of free space and $\Delta\varepsilon_{PMO}$ is the anisotropy of the relative dielectric constants of the PMO particles, this driven process could be considerably faster, of order hundreds or even tens of milliseconds. In principle, one may be able to separate this direct rotational relaxation (which has an E^2 behavior) from the electroclinic process (which is linear in E), but two factors work against this. First, the available voltage range is limited due to onset of electrohydrodynamic instabilities of the liquid crystal at higher voltages [19] and the much smaller signal-to-noise ratio at the lower frequencies where rotational diffusion could come into play. Second, PMO rotation can result in smectic layer breaking, thereby coupling processes at ω and 2ω and confounding the analysis. Nevertheless, we believe that the observed low frequency behavior is not a true electroclinic effect associated with the chirality of the PMO, but rather involves a very low frequency artifact of the PMO's shape and pore arrangement. Earlier measurements [11] in which the chirality was removed by plugging the pores with a surfactant were performed at much higher frequencies and would not have been sensitive to this low frequency artifact.

We now consider the role played by the liquid crystal-filled chiral pores in the electroclinic signal. Owing to the small pore diameter, ~ 2.5 nm, we would expect that the liquid crystal molecules in the pores would become conformationally deracemized, and that the chiral strength of

the liquid crystal would be approximately uniform inside the pores [22]. In this case we return to Eq. 3, and note that the wavevector q would be of order 10^9 m^{-1} for the small pore diameter. Here the Kq^2 term can be comparable to D even far above T_{AC} where D is large. But as before, close to T_{AC} the Kq^2 term would be much larger than D, resulting in a relaxation process having a characteristic frequency Kq^2 / η , which is of order 10^9 to 10^8 s^{-1} for $\eta \sim 0.01$ to 0.1 kg m^{-1} s^{-1}. Although these frequencies are well beyond the capabilities of our experimental equipment, the data in Fig. 5 show almost a complete decay of signal for $\omega \sim 10^6$ sec^{-1} close to the bulk Sm-*A* – Sm-*C* transition, which suggests that the liquid crystal-infiltrated pores' contributions to the observed electroclinic signal are small compared to the bulk liquid crystal contribution in this temperature range. That is, the electrooptic effect apparently is dominated by the behavior of the bulk liquid crystal *outside* the pore, such that the chiral pores induce a conformational deracemization of the liquid crystal inside the pores, which in turn causes a deracemization of the liquid crystal in the region at which the pore terminates at the PMO / bulk liquid crystal boundary. It is this region, when driven by an electric field, that couples elastically to the bulk liquid crystal. We should remark that the pores' tiny diameters also suppress the Sm-*A* to Sm-*C* phase transition within the pores, and thus suppress the pretransitional behavior associated with Eq. 3 [1].

4. Summary

The advent of chiral periodic mesoporous organosilica materials presents many opportunities for technological development, especially involving composite materials. Our results reveal a complex electrooptic response when the PMO is mixed with a liquid crystal. Not only do we observe a low frequency response that we believe is an artifact of the electric field coupling to the PMO colloids themselves, but also the apparent absence of a high frequency relaxation that would be characteristic of an electroclinic response within the PMO's pores. This suggests that the

observed electroclinic response comes overwhelmingly from the chiral-induced region outside the chiral pores and the subsequent viscoelastic response of the bulk liquid crystal outside of this region, and is templated by the liquid crystal within the chiral pores of the PMO materials.

Acknowledgments IRN and CR were supported by the U.S. National Science Foundation's Condensed Matter Physics program under grant DMR-1505389. CMC, KM, and RPL were supported by the Natural Sciences and Engineering Research Council of Canada (NSERC) and the Canada Foundation for Innovation (CFI).

Figure Captions

1. TEM image of PMO showing the 2D hexagonally ordered porous mesostructured.

2. Chemical structures of: **1)** liquid crystal 9OO4, **2)** (S) chiral binaphthyl monomer, **3)** 4,4'-bis-(triethoxysilyl)biphenyl, and **4**) chiral dopant CB15.

3. Electroclinic response $I_{ac}/4I_{dc}$ *vs.* applied voltage for the **CB15 / 9OO4** sample at three temperatures in the Sm-*A* phase.

4. Electroclinic response $I_{ac}/4I_{dc}$ *vs.* angular frequency ω for the **CB15 / 9OO4** sample at four different values of ΔT. Here the applied voltage was fixed at 7 V.

5. Electroclinic response $I_{ac}/4I_{dc}$ *vs.* angular frequency ω for the PMO / **9OO4** sample at four different values of ΔT. Here the applied voltage was fixed at 7 V.

6. Electroclinic response $I_{ac}/4I_{dc}$ *vs.* angular frequency ω for the **CB15 / 9OO4** sample at two different values of ΔT with a two-parameter fit to Eq. 3 and neglecting the Kq^2 term.

References

[1] Crawford, G.P.; Žumer, S. **Liquid Crystals in Complex Geometries**, Taylor & Francis, London (1996)

[2] Wehrspohn, R.B; Kitzerow, H.-S.; Busch,K. **Nanophotonic Materials**, Wiley-VCH, Weinhem (2008)

[3] Tsoi, W.C.; O'Neill, M.; Aldred, M.P.; Kitney, S.P.; Vlachos, P.; Kelley, S.M. *Chem. Mater.* **2007**, *19,* 5475 - 5484

[4] Levitsky, I.A.; Euler, W.B.; Tokranova, N.; Xu, B.; Castracane, J. *Appl. Phys. Lett.* **2004,** *85*, 6245 - 6247

[5] Ide, A.; Voss, R.; Scholz, G.; Ozin, G.; Antonietti, M.; Thomas, A. *Chem. Mater.* **2007,** ***19***, 2649 - 2657

[6] Inagaki, S.; Guan, S.; Yang, Q.; Kapoor, M.P.; Shimada, T. *Chem. Commun.* **2008**, 202 - 204

[7] Brethon, A.; Hesemann, P.; Rejaud, L.; Moreau, J.; Man, M. *J. Organomet. Chem*. **2001,** ***627***, 239 -248

[8] Wang, P.; Liu, X.; Yang, J.; Yang, Y.; Zhang, L.; Yang, Q.; Li, C. *J. Mater. Chem.* **2009,** *19*, 8009 - 8014

[9] MacQuarrie, S.; Thompson, M.P.; Blanc, A.; Mosey, N.J.; Lemieux, R.P.; Crudden, C.M. *J. Am. Chem. Soc.* **2008,** ***130***, 14099 - 14101

[10] Giese, M.; De Witt, J.C.; Shopsowitz, K.E.; Manning, A.P.; Dong, R.Y.; Michal, C.A.; Hamad, W.Y.; MacLachlan, M.J. *Appl. Mat. Interfaces* **2013,** *5*, 6854 - 6859

[11] Jayalakshmi, V.; Wood, T.; Basu, R.; Du, J.; Blackburn, T.; Rosenblatt, C.; Crudden, C.M.; Lemieux, R.P.; *J. Mater. Chem.* **2012,** *22*, 15255 - 15261

[12] MacLean, M.W.A.; Read, L.M.; Wu, X.; Crudden, C.M. *Chem. Asian J.* **2015,** *10*, 70 - 82

[13] Zhang, L.; Liu, J.; Yang, J.; Yang, Q.; Li, C. *Chem. Asian J.* **2008,** ***3***, 1842 - 1849

[14] T.Y. Zhuang, J.Y. Shi, C. Ma, and W. Wang, *J. Mater. Chem.* **2010**, *20*, 6026 - 6029

[15] Wang, P.; Yang, J.; Liu, J.; Zhang, L.; Yang, Q. *Microporous Mesoporous Mater.* **2009,** ***117***. 91 - 97

16 Kuschel, A.; Sievers, H.; Polarz, S.; *Angew. Chem. Int. Ed.* **2008**, *47*, 9513-9517

[17] Raynes, E.P. *Liq. Cryst.* **2006**, *33*, 1215 - 1218

[18] Garoff, S.; Meyer, R.B.; *Phys. Rev. Lett.* **1977**, *38*, 848 - 851

[19] Seki, T.; McEleney, K.; Crudden, C.M. *Chem. Commun.* **2012**, *48*, 6369-6371

[20] Andersson, G.; Dahl, I.; Keller, P.; Kuczynski, W.; Lagerwall, S.T.; Skarp, K.; Stebler, B. *Appl. Phys. Lett.* **1987**, *51*, 640 - 642

[21] DeGennes, P.G.; Prost, J. **The Physics of Liquid Crystals**, Clarendon, Oxford (1994)

[22] Delaye, M. *J. Phys. (Paris) Colloq.* **1979**, *40*, C3-350 – C3-355

[23] Li, Z.; Akins, R.B.; DiLisi, G.A.; Rosenblatt, C.; Petschek, R.G. *Phys. Rev. A* **1991,** *43*, 852 - 857

[24] We also note that a very weak and slow decay process at $\omega \sim 10^3$ s^{-1} was observed at temperatures> T_{AC} + 2° C. Closer to T_{AC} this was overwhelmed by the much larger (and growing) mode corresponding to $d\theta/dE$. This very weak process is beyond the scope of this work, and we concentrate on the dominant processes close to T_{AC}.

[25] Berardi, R.; Kuball, H.-G.; Memmer, R.; Zannoni, C. *J. Chem. Soc., Faraday Trans.* **1998,** *94*, 1229 - 1234

26 Nemitz, I.R.; Rosenblatt, C.; to be published

27 Ciesla, U.; Schüth, F.; *Microporous Mesoporous Mater.* **1999**, *27*, 131-149

28 Wegener, W.A.; Dowben, R.M.; Koester, V.J.; *J. Chem. Phys.* **1979**, *70*, 622-632

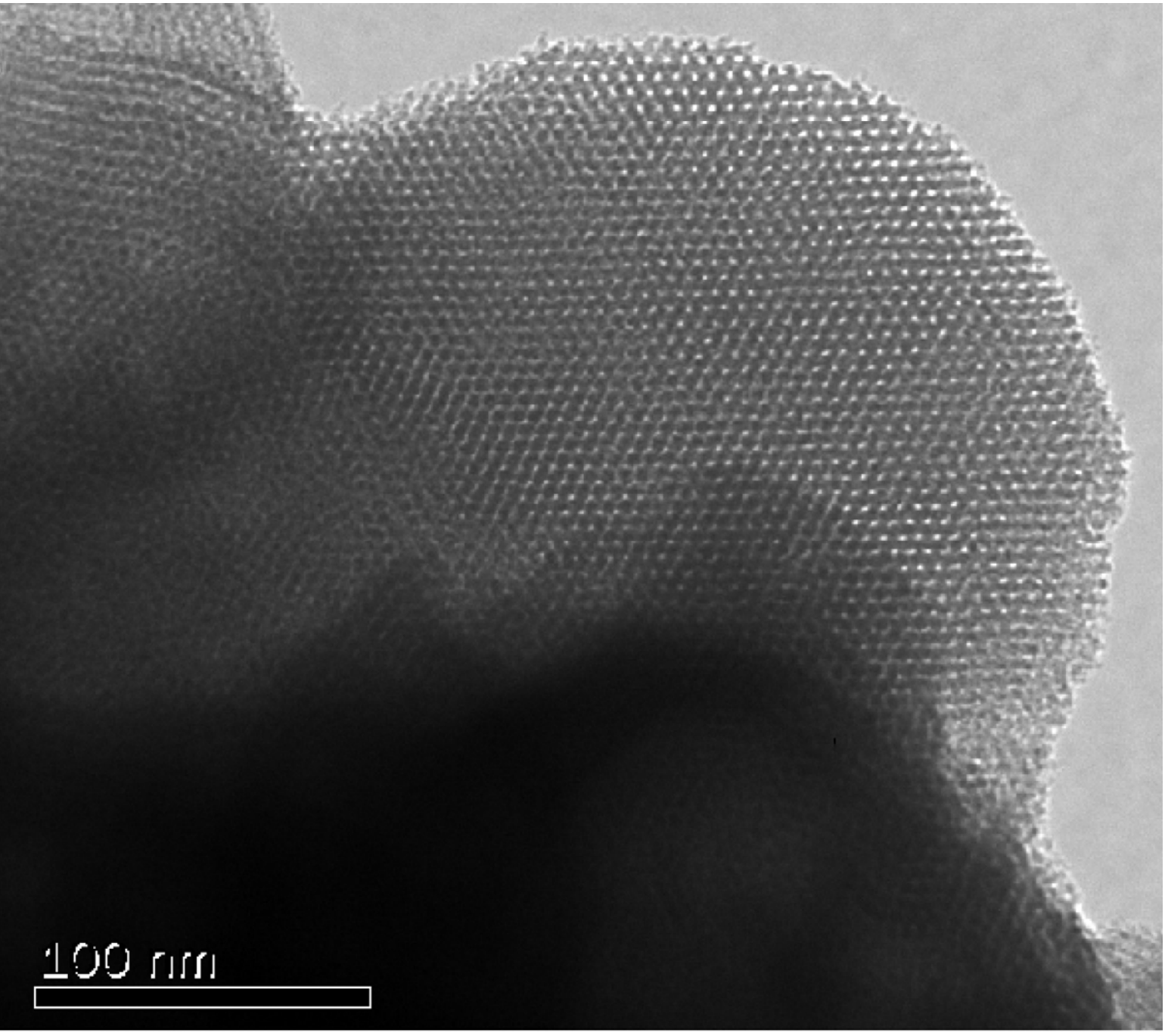
100 nm

1

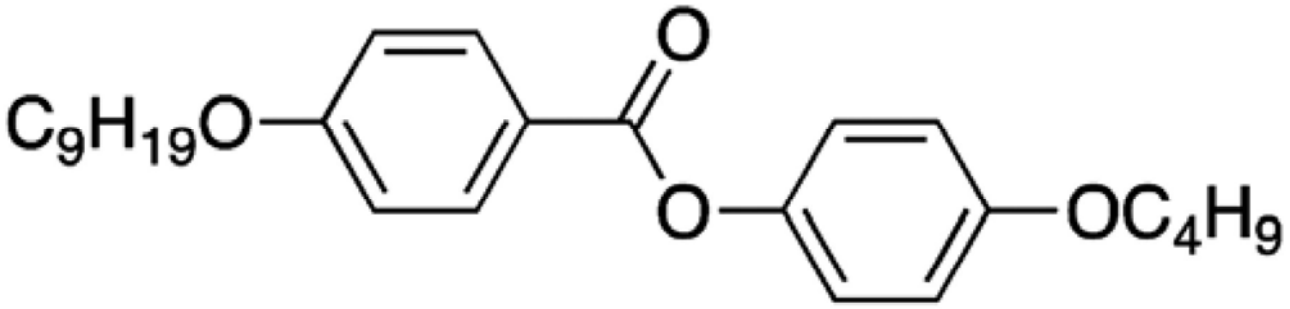

2

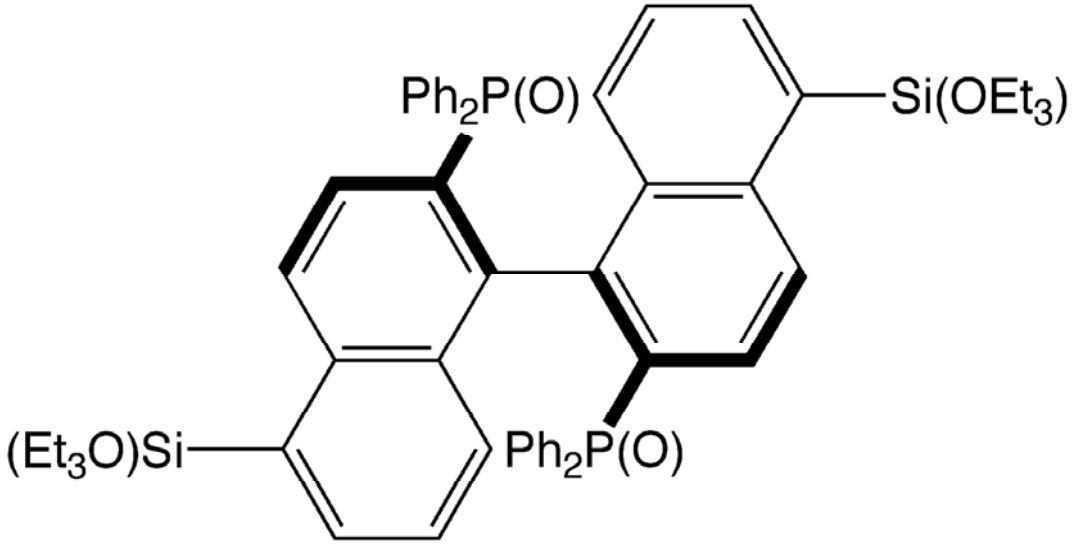

3

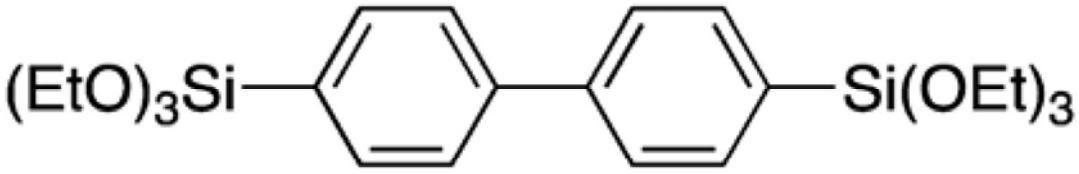

4

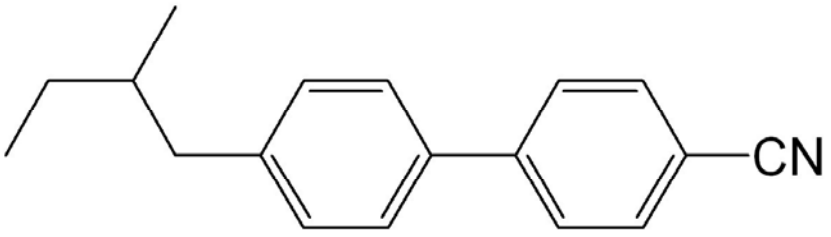

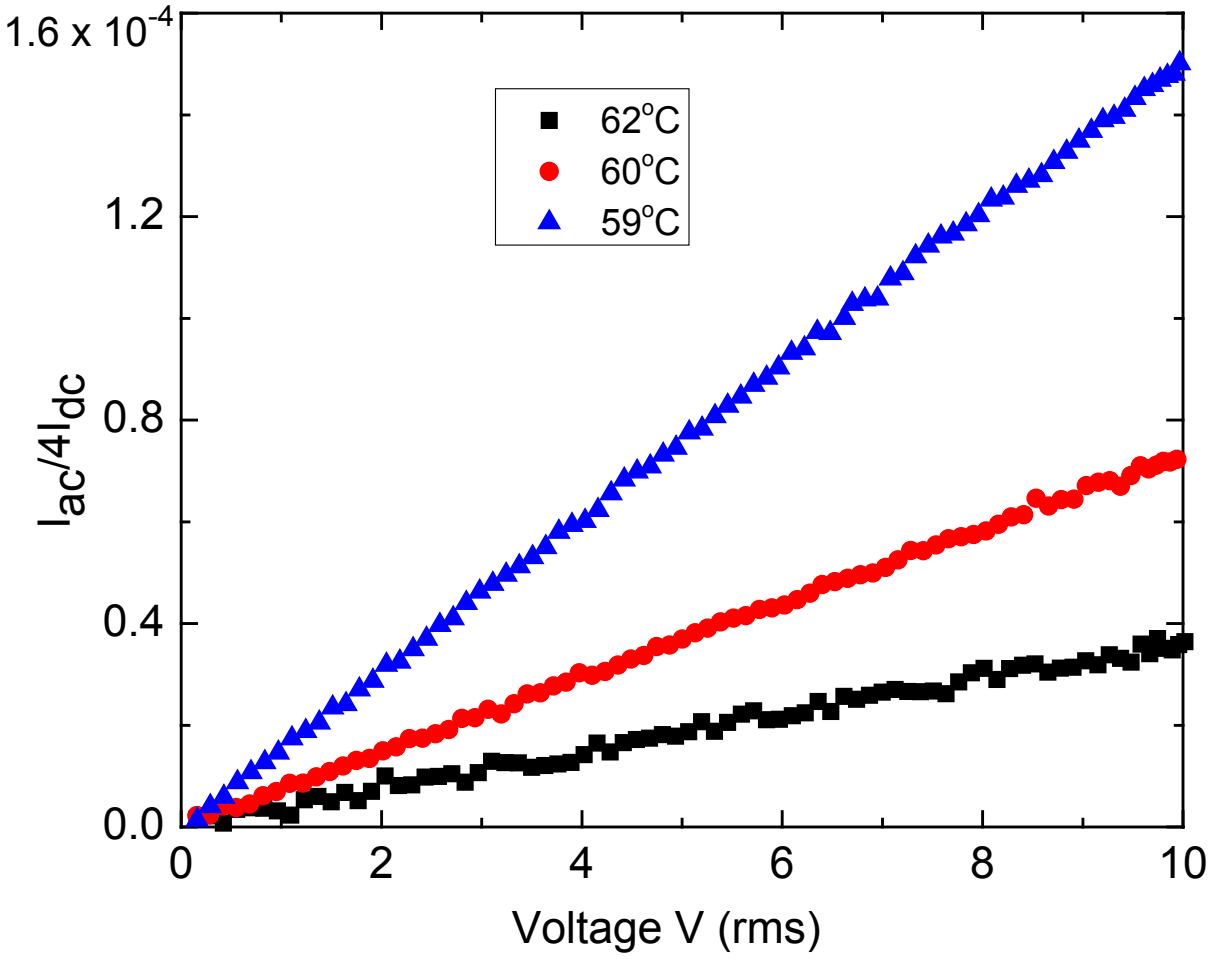
1.6 x 10-4
1.2
0.8
0.4
0.0
Iac/4Idc
0
2
4
6
8
10
Voltage V (rms)
62°C
60°C
59°C

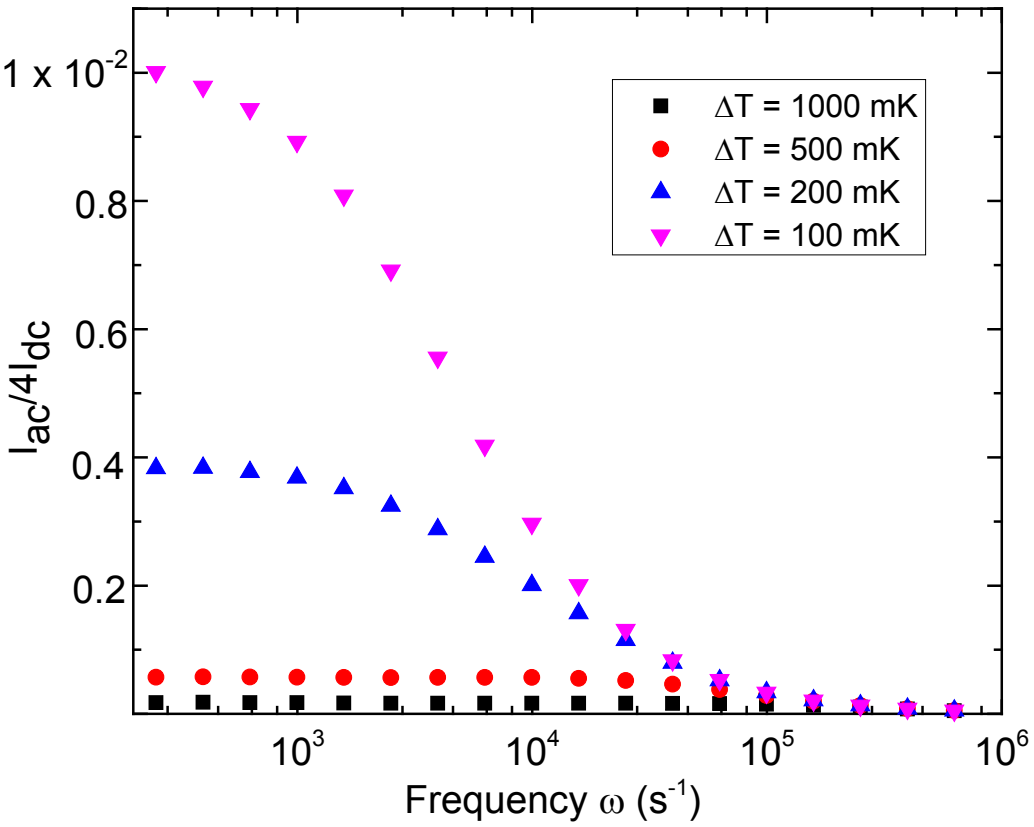
1 x 10-2
0.8
0.6
0.4
0.2
Iac/4Idc
ΔT = 1000 mK
ΔT = 500 mK
ΔT = 200 mK
ΔT = 100 mK
10^3
10^4
10^5
10^6
Frequency ω (s-1)

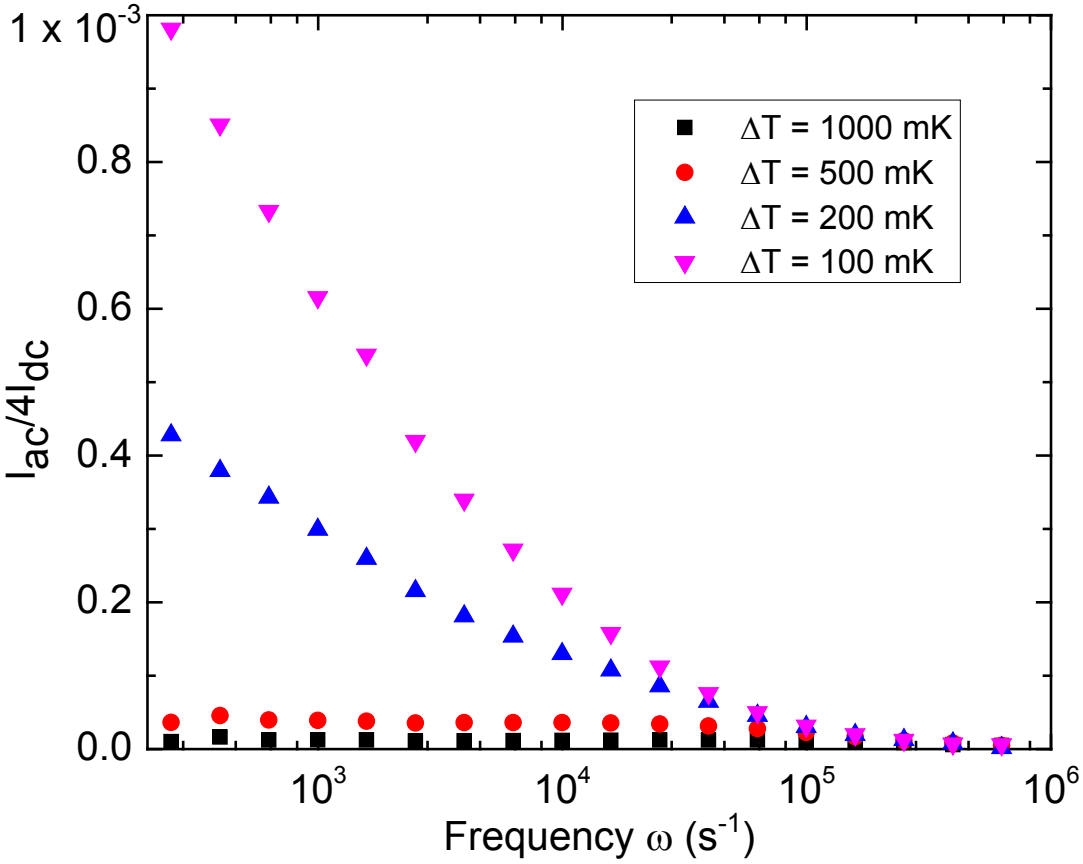
1 x 10-3
0.8
0.6
0.4
0.2
0.0
Iac/4Idc
ΔT = 1000 mK
ΔT = 500 mK
ΔT = 200 mK
ΔT = 100 mK
10^3
10^4
10^5
10^6
Frequency ω (s-1)

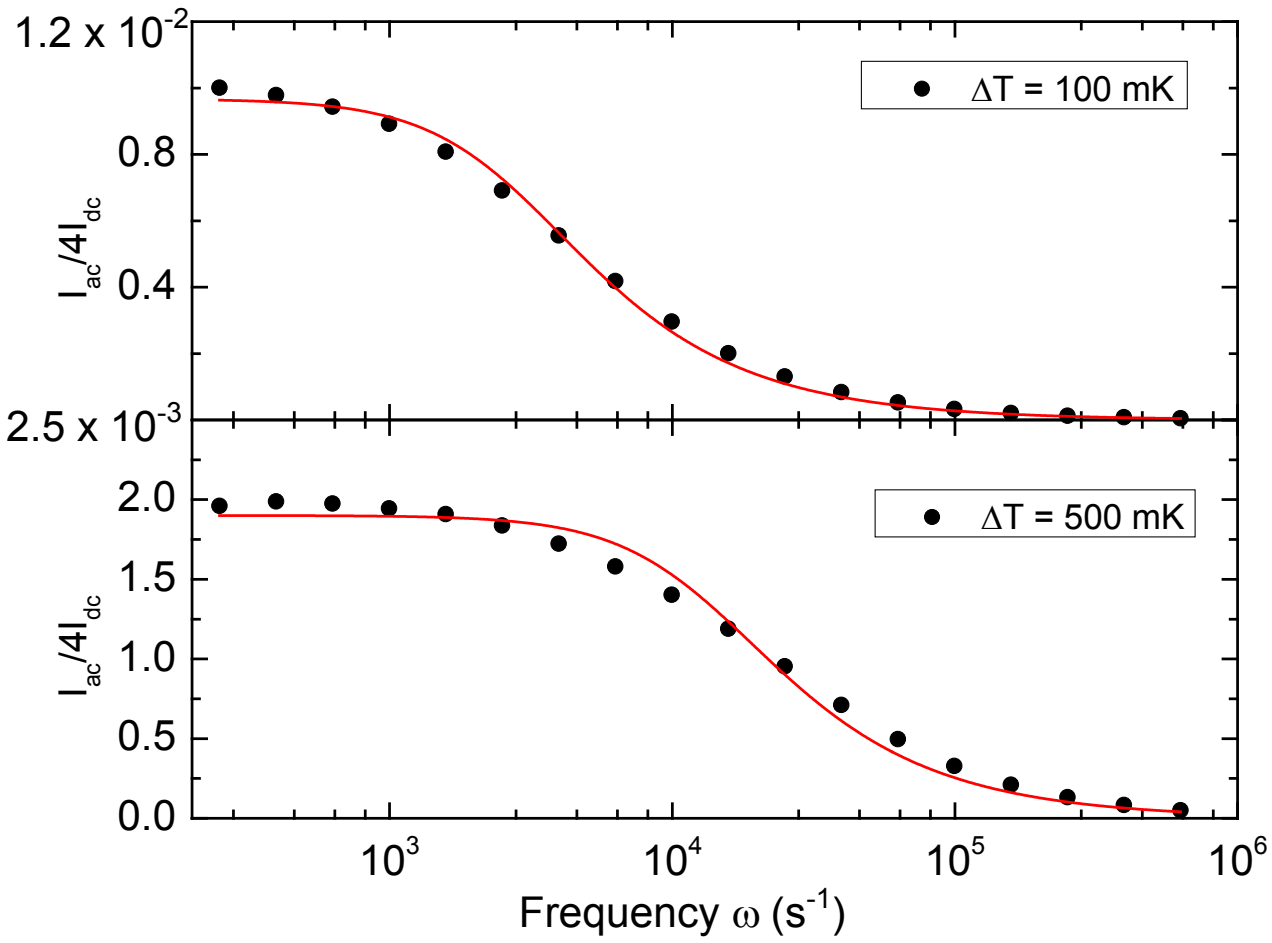
1.2 x 10-2
0.8
0.4
Iac/4Idc
ΔT = 100 mK
2.5 x 10-3
2.0
1.5
1.0
0.5
0.0
Iac/4Idc
ΔT = 500 mK
10^3
10^4
10^5
10^6
Frequency ω (s-1)